International Journal of Scientific Research in Science, Engineering and Technology

Print ISSN - 2395-1990
Online ISSN : 2394-4099

OPEN ACCESS

Available Online at : www.ijsrset.com
doi : https://doi.org/10.32628/IJSRSET2310543

Effect of Input Layer Signal Polarization on the Dynamics of Optical Neural Networks

Mariam R. Dhyaa* and Ayser A. Hemed

Department of Physics, College of Education, Mustansiriyah University, Baghdad, Iraq

*Corresponding author : mariamraaed1998@uomustansiriyah.edu.iq

ARTICLEINFO

Article History :

Accepted: 05 Oct 2023
Published: 30 Oct 2023

Publication Issue :

Volume 10, Issue 5
September-October-2023

Page Number :

279-293

ABSTRACT

The polarization encoding-based optical validation and security verification approach is provided in this paper. This technique involves simulating information optically and bonding it to a polarization-encoded mask, such as a biological order or a reaction. The linear polarizers that make up the polarization-encoded mask are positioned at random. The polarization-encoded signal is the name given to this composite signal. In this simulation study, a primary optical neural network adapting a light brain technology is proposed theoretically based on a feed-forward model. Calibration of the nonlinear behavior in such a network is assumed by a semiconductor laser of the Distributed Feedback (DFB) type. Four laser networks are constructed as three influencers, followed by one embedding laser followers. Each of the influencer's lasers has a different wavelength frequency and polarization (30-60–90) degree, respectively, and then combines the signal with WDM for the last laser. With each value, from the last values, of the polarization effect after this effect, the results indicated that these values would present the greatest weight of spikes and chaotic behavior for the uploaded virtual message.

Keywords : Distributed Feedback, WDM, Optical Validation

I. INTRODUCTION

Deep neural networks have recently been used to solve a variety of issues, including those relating to image analysis, natural language processing, game play, physical chemistry, and medicine. But this is hardly a brand-new field. Deep learning's theoretical foundations have been developed over many years [1]. Optical neural networks are the child of neural network theory and optical information processing. The remaining portion of this special issue is devoted to optical computing. Layers are typically used to organize neural networks in both biology and technology. Such units can be linked from one layer to the next, backward, or even laterally in a very basic feed-forward, single-layer neural network. The outputs of one layer might become the ultimate outputs or the inputs of another. Zero interconnect weights are permitted [2]. Due to their extremely high signal bandwidths, extremely low latencies, and

flexibility, optical hardware systems are particularly desirable for computing and signal processing [3]. Because of their compact size, great efficiency, and capability to directly modulate at gigabit per second rates, semiconductor lasers play a significant role in optical communication systems. [4]. However, the performance of conventional machine learning algorithms is far from ideal when it comes to human information processing processes (such as voice and vision). The idea of deep learning algorithms was first proposed in the late 20th century and was inspired by the complex hierarchical structures of human speech perception and production systems. Since Hinton presented the deep belief network (DBN), a unique deep structured learning architecture, in 2006, significant advances in deep learning have been made. Using neurons to generate real-valued activations is necessary to build a typical neural network (NN), and by modifying the weights, the NNs function as intended. However, training a NN might involve lengthy causal chains of computing processes, depending on the challenges [5]. DFB lasers were created to enhance the selection of the longitudinal mode. Using a grating that has been etched, the feedback required for the lasing activity is dispersed over the cavity length, causing the thickness of the active layer to change regularly along the cavity length. Up until there is no light at the rear of the grating, the rating reflects a little light over each section of the grating. The use of DFB lasers in optical transmission systems is by far their most prevalent application [6].
Lazarevic and Obradoric (2001) proposed a pruning algorithm to get rid of redundant classifiers in order to find a highly diverse set of accurate trained networks. Zhou et al. (2001) described a selective constructing approach for ensembles, and Fu et al. (2005) proposed clustering-based selective neural network ensembles. A particularly effective method for combining the results of several independently trained neural networks into a single forecast is called a neural network ensemble [7]. An artificial neural network (ANN) is a model of the human brain. A normal brain can learn new things and adapt to unfamiliar situations. The ability of the brain to deduce its own conclusions from confusing, illegible, and incomplete input is truly remarkable.

Neurons are the processing components that make up an artificial neural network. An artificial neuron's objective is to replicate the structure and operation of a genuine neuron. A neuron has two inputs (dendrites) and one output (a synapse through an axon). The function of the neuron governs how it is triggered [8]. Several research, including Refs. [9] [10] [11] [12] proposed a connection between optical communication systems and optical neural network.
Three fundamental elements are of relevance when building a functioning model of biological neurons. The synapses of neurons are first represented as weights. The weight value measures the strength of the link between the input and the neuron. Inhibitory connections are represented by negative weight values, and excitatory connections are represented by positive weight values (Heikin)as shown in the following figure (Fig. 1) [13].

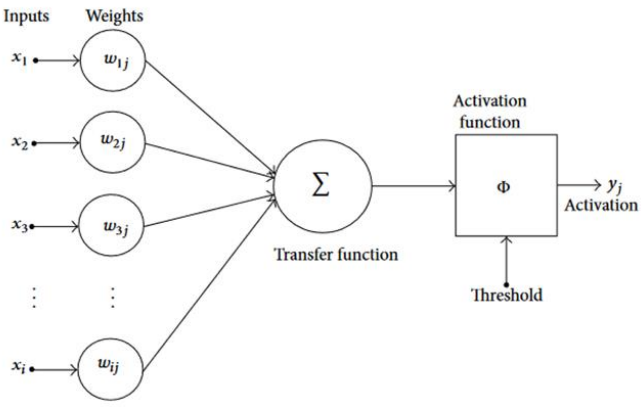

Figure 1. Mathematical Model [13]

Along with inputs, a bias is also introduced to the neuron; typically, the bias value is initialized to 1. The signal is connected to the weight. The intensity of the signal is calculated as the product of weight and input. A neuron has a single output while having several

inputs from various sources [8]. A technological innovation in intelligence is neural networks [14].

THEORITICAL CONCEPTS

Due to changes in kilometers, frequency, minimum bit error rate, eye height, threshold, and dispersion, as well as their influence on communication, managing large amounts of data is challenging in optical fiber networks. It required a system that could manage the massive volume of data with ease and forecast the system's performance quickly and affordably. The best option for this is an artificial neural network. Artificial neural networks are man-made networks that resemble the human brain; this is why they are dubbed "artificial." ANN models can manage connections between input and output data that are not linear [15]. The terms "artificial neural networks," "artificial neural systems," "parallel distributed processing systems," and "communication systems" are also used to refer to artificial neural networks [16]. In-depth research has recently been done on DFB lasers to stabilize the longitudinal modes [17]. In 1994, the fiber DFB laser saw its maiden demonstration [18]. A semiconductor laser's functioning presents a very challenging modeling challenge [19]. Due to its tiny line width, reliable single longitudinal mode operation, small in-fiber construction, adaptable and precise wavelength selection in production, and simple wavelength adjustment, fiber DFB lasers are desirable tools for both communications and sensing applications [20]. Quarter-wave-shifted distributed feedback (QWS-DFB) lasers' threshold spectral features are examined in relation to the impacts of a localized impurity. Long-haul communications networks now heavily rely on QWS-DFB lasers. Single-mode operation is guaranteed to occur precisely at the Bragg frequency by the built-in phase shift [21]. For flexibility in pumping settings and pump redundancy, a number of DFB fiber lasers can be arranged in a parallel array. Additionally, they are capable of steady operation in a single longitudinal mode and polarization, and passive stabilization enables precise control of the emission wavelength. They are naturally compatible with fiber. They also have low relative intensity noise (RIN) and low phase noise [22]. Using distinct wavelengths for the transmission of numerous information sources, dense wavelength division multiplexing (DWDM) is a method that enables multiplexing of several optical carrier signals on a single optical fiber. Compared to temporal division, it is a more effective source of transmission [23].

One of the fundamental characteristics of electromagnetic waves is polarization, which transmits important information during signal transmission and delicate measurements [24]. The primary concern in the optical communication system to address dispersion issues is dispersion compensation technology. To compensate for losses caused by single-mode fiber, optical amplifiers and erbium-doped fiber amplifiers (EDFA) are utilized. Another form of dispersion produced during the production of optical fiber is polarization mode dispersion (PMD), which results from geometrical variations in the concentricity core or cladding layer. The PMD surpasses with fiber cable expansion as the optical signal travels via single-mode fiber. The crucial need is to use a compensating strategy to reduce polarization mode dispersion [25].

The transfer matrix technique and other computer programs are frequently used in the investigation and modeling of the DFB laser's properties [26]. It is commonly anticipated that optical processing would eventually need to be carried out entirely via optical means as the demand for higher and higher bandwidths in telecommunication networks grows [27]. The creation of novel devices that enable quick and all-optical control of the state of polarization (SOP) of a light beam has drawn the attention of several research groups in response to the development of ultra-high bit-rate and transparent optical communication systems and the associated complex modulation formats and signal processing issues. In fact, to get around the electrical bottleneck and go beyond what the present electronic feedback systems can do [28]. The spin sublevels of the lasing transitions

between the conduction and valence bands of the semiconductor material are where the polarization of laser light, which is of a quantum nature, first appears. When a linear polarization (LP) state is taken into account, there are two linear components: one with very little intensity (the non-lasing component), which has a mean power level P_{ni}, and one with almost the whole intensity (the lasing component), which captures almost the entire intensity [29]. The best method for mastering or controlling the state-of-polarization (SOP) of light in fiber-based systems is to use an opto-electronic polarization tracker. These devices often rely on linear polarization changes, partial diagnostics, active feedback loop control, and sophisticated algorithms. Record polarization tracking speeds have been attained using this time-tested method, with commercially available equipment reaching several Mrad/s [30].

The DFB laser is primarily a Fabry-Perot laser with a grating array above the active layer, according to the Optisystem program model. The DFB is set up so that when quarter wave shift at the center is disabled, there will be two dominant modes at equal distances on either side of the Bragg wavelength (note that owing to flaws in real DFB lasers, typically one of these modes will be more prominent). When quarter wave shift at center is enabled, one dominant mode will exist exactly at the Bragg wavelength (in this example). Equation for laser internal current I(t) is given as:

$$I(t) = I_{DC} + I_{in}(t) \times I_{PK} \quad (1)$$

where $I_{in}(t)$ is the input signal current, I_{DC} is the parameter Bias Current and I_{Pk} is the parameter modulation peak current. If the parameter bias current and modulation peak current have zero values, the internal current is given by $I_{in}(t)$ only. The modulation dynamics of the DFB laser are modeled by the multimode rate equations which describe the relation between the carrier density N(t), photon densities $S_i(t)$, and optical phases $\varphi_i(t)$:

$$\frac{dN(t)}{dt} = \frac{I(t)}{q.V} - \frac{N(t)}{\tau_n} - \sum_i \left[G_i \,.\, (N(t) - N_t . \frac{1}{(1 + \sum_j \varepsilon . s_j(t))} . s_i(t) \right] \quad (2)$$

$$\frac{dS_i(t)}{dt} = G_i . (N(t) - N_t) . \frac{1}{(1 + \sum \varepsilon . s_i(t))} . s_i(t) - \left(\gamma_p . s_i(t)\right) + \frac{\Gamma \beta N(t)}{\tau_n} + k_c . s_{ext}(t) \quad (3)$$

$$\frac{d\phi_i(t)}{dt} = \frac{1}{2} . \alpha [\Gamma . G_i . (N(t) - N_t) - \gamma_P] \quad (4)$$

where symbols in last equations are given in the following table 1.

Table 1. Definitions for used symbols [31] [9].

Symbol	Meaning
ε	gain compression factor
N_t	carrier density at transparency
β	spontaneous emission factor
Γ	mode confinement factor
V	active layer volume
γ_p	cavity loss
τ_n	carrier lifetime
α	line-width enhancement factor
$S_{ext}(t)$	optically injected signal
K_c	photon density coupling factor for the injected optical signal

The DFB structure is modeled by alternating each transmission line section with "high" or "low" impedances (for the quarter wave shift, the two most central layers will have the same impedance) which will generate corresponding scattering matrices at each node [32] [31] [9].

The prerequisite to the application of any machine learning algorithm is data collection and formatting. Without suitably formatted data, the algorithm cannot be used to its fullest extent and may provide spurious and undesirable results or even outright reject the data being provided [23]. It has been created to address the needs of research scientists, optical telecom engineers, system integrators, students, and a wide variety of other users. Optisystem satisfies the demand of the evolving photonics market for a powerful yet easy-to-use optical system design tool. Optisystem enables users to plan, test, and simulate (in both the time and frequency domains). Furthermore, it includes visualization tools for doing observations and analysis on several signal positions between the first and last outputs. Signal generators are connected due to the necessity of laser operation via the program.

SIMMULATION SET-UP

To mimic the DFB lasers, split-step time-domain dynamic modeling is employed [33]. simulation set-up is described in shorthand in the architecture given in Fig. 2. The investigated network consists of four DFB-type laser sources; three of these lasers correspond to influencers, and the fourth is the follower one. Each of those influencers' signals has a certain wavelength and polarization, such that it differs from the others. Outputs for all those sources are going to be collected by using a WDM before insertion into the follower. The weight of each of the influencing lasers is measured by the follower spectrum. The exact set-up is shown in figure 3, in which a polarization meter is also used to display the total signal power in the visualizers in order to analyze the result. The polarization properties are measured at a user-defined frequency and bandwidth. This visualizer allows the user to calculate the average polarization state of the optical signal, including the degree of polarization (DOP), differential group delay (DGD), Stokes parameters, azimuth and ellipticity. It is used to calculate the delay between polarizations X and Y, i.e., birefringence. To test the communication system, information such as a frequency message must be uploaded. A frequency generator is used to send a signal from influencers; at the beginning, these messages were set to 0 Hz only to ensure the laser source was operating according to Optisystem code. The wavelengths for lasers DFB1, DFB2, and DFB3 are 1549, 1550, and 1551 nm, respectively. Then the signal from each of them goes to the ideal linear polarizer with values of 30, 60, and 90 degrees, respectively, in order to make the polarization alignment. The output signal is collected by WDM Mux with frequency channels equal to the frequency of the influencing lasers.

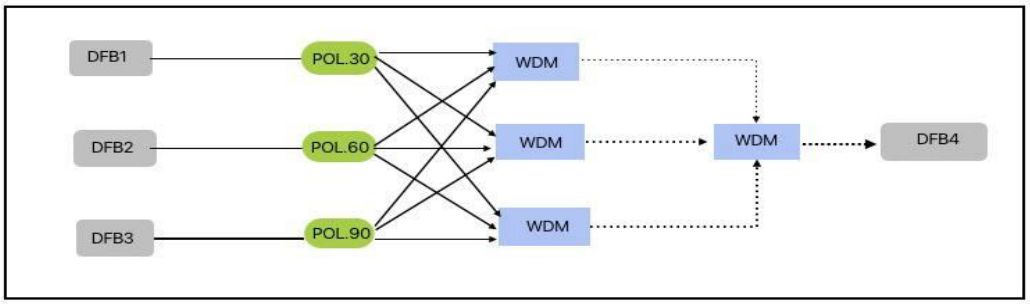

Figure 2. Architecture for the feed-forward simulation set-up experiment.

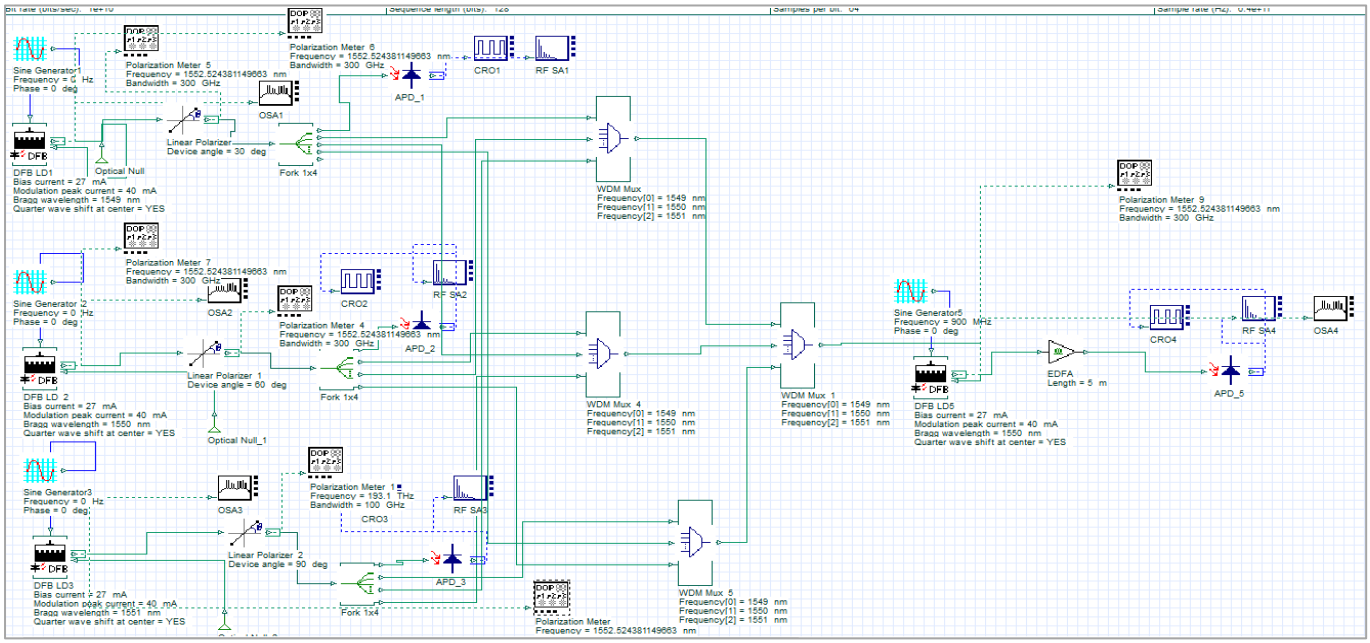

FIGURE 3. Simulation set-up for the feed-forward simulation set-up with a unidirectional chaotic modulation. OSA is the optical spectrum analyzer, CRO is the Oscilloscopes visualizers, RFSA are the radio frequency spectrum analyzers, EDFA is the Erbium doped fiber amplifiers.

II. RESULTS AND DISSCUSSION

Influencer Lasers Dynamics

Observations of the dynamics of each influencer are carried out. First, second, and third influencer lasers have different wavelengths in order to distinguish each signal weight in the follower. Furthermore, linear polarization is set with different values for the incoming signals from those lasers. As given in Fig. 4, observed dynamics are: time series behaviors (part a from the figure), number of peaks (calculated from the RF spectrum in part (b) from the figure), peak wavelength λ_p from OSA (part (c) from the figure). The observed coordinates for those peaks are listed in Table 3. It is noticed that when the polarization value is 90 degrees, the signal becomes a straight line. The explanation is that the polarization module has been canceled, so there are no peaks. It is noticed from last table that dynamics for each influencer is different in all spaces that has been recorded. This is due to impact of polarization with which signals details are blocked in part of it and permitted in the others. This is based on concept of birefringence in optical fibers i.e. degeneracy for one linear polarization with respect to the other with a beat length as reported for example in Ref. [34]. Both polarization selection techniques are used to solve the problems of multiplexing and demultiplexing in optical communications systems related to optical neural networks. In Tables 1 and 2, the rating of the measured forces against the polarization values in the network is shown.

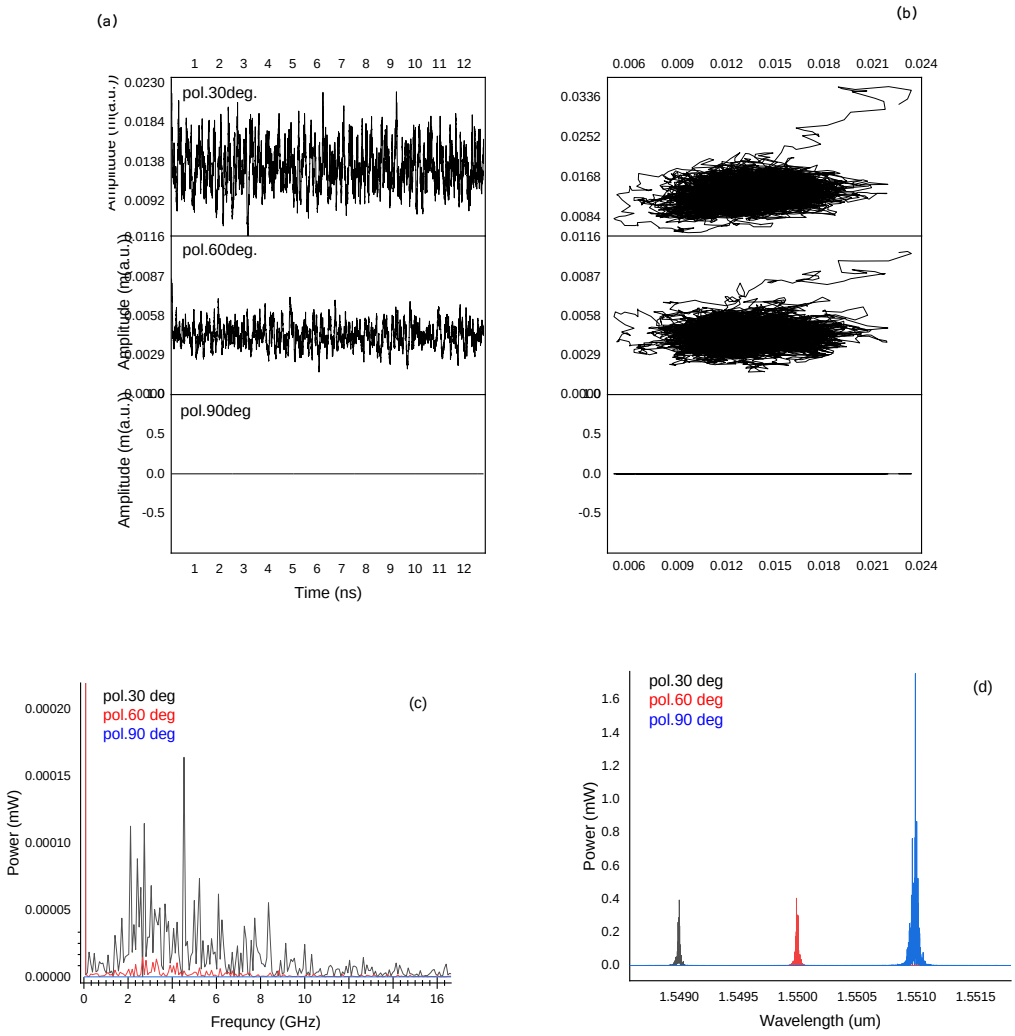

FIGURE 4. Influncers observed dynamics. (a) Time series (b) Phase space (c) Frequency spectrum and (d) Optical spectrum.

Table 2. Classification for measured powers against polarization values in the network.
DOP: degree of polarization, and S_o power.)

No.	DOP (%)	S_O (dBm)
LD1	100	-41.793
LD2	100	-34.567
LD3	100	-100

The selected polarization values for the influencers are three in comparison with the fourteen reported in simulation Ref. [35] or the N number reported in Ref. [36]. Both polarization selection techniques are used to solve the problems of multiplexing and demultiplexing in optical communications systems related to optical neural networks.

Table 3. Classification for measured powers against selected polarization values in the network.

No.	DOP (%)	S_O (dBm)
POL.30	100	-40.544
POL.60	100	-40.589
POL.90	100	-100

Table (4). Measurements for FWHM and Peak wavelength against Polarization for signal the influencer given in figure (4).

Influencer wavelength (nm)	Pol. (deg.)	Dynamic (GHz)	No. of peaks	λ_p(um)	
				Lambda (um)	Power (mW)
DBF1 (1549)	30	0-10	15	1.54900057	0.394915893
DBF2 (1550)	60	0-15	13	1.54999726	0.40401811
DBF3 (1551)	90	non	0	1.55099042	1.76511036

Effect of DFB1 in overall summed signal

Signals that have come from each individual influencer will sum or mix with those that came from the remaining influencers in order to meet the model reported by that has been shown in Fig. 2. One influencer of on overall resulted signal is observed and shown in Fig. 5. Effect of DFB1 polarization on the last follower laser was measured regardless of DFB2 and DFB3. Polarization values were; (10-20-30) degree while the two remaining lasers polarization is set with constant values (60-90), respectively. It is noticed that values as recorded in Table 5 that the number of peaks decreases with increasing polarization.

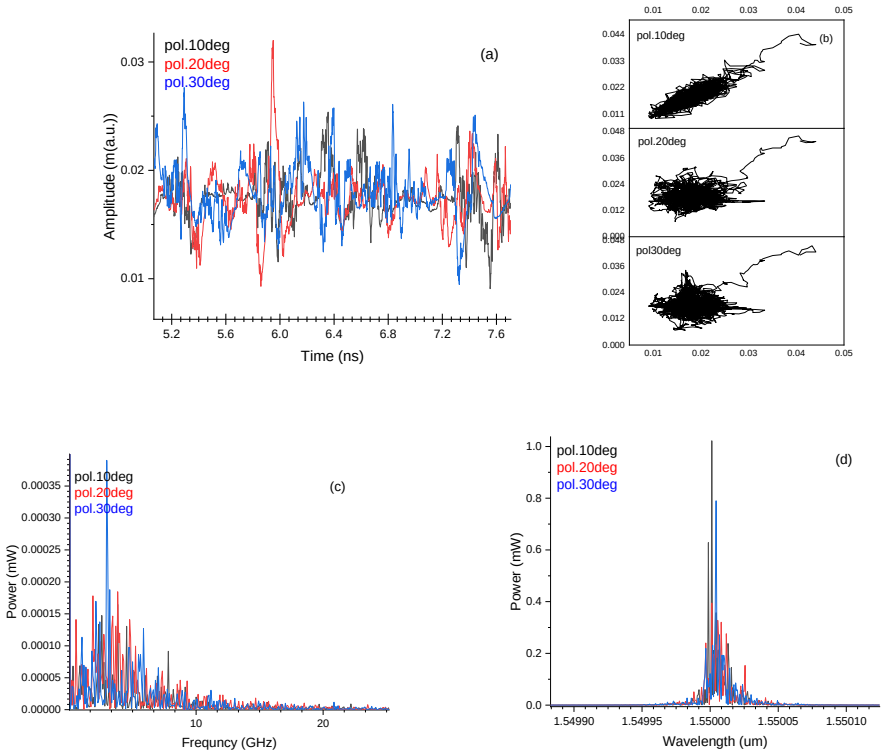

FIGURE 5. Dynamics for summed signal with DFB1 polarzation variation.
(a) Time series (b) Frequency spectrum (c) optical spectrum and, (d) phase space.

Table (5). Measurements for FWHM and Peak wavelength against phase shift for received signal from the influencer given in figure (5).

Polarization (degree)	Dynamic range (GHz)	No. of peaks	λ_p (um)	
			Lambda (um)	Power (mW)
10	0-8	21	1.5499992 1.5500007	0.61860217 1.02623134
20	0-14	16	1.54999715 1.55000576 1.55000066	0.236595788 0.323166529 0.394705831
30	0-7	7	1.55000412 1.55000486	0.725510707 0.79037722

Effect of DFB2 in overall summed signal

As it was carried out in the last section, the effect of DFB2 on the last follower laser was measured regardless of DFB1 and DFB3. By changing the polarization three times (40-50-60) and keeping the polarization of the first and third lasers at 30–90 degrees, respectively. Observed dynamics are given in Table 6. In which the number of peaks decreases with increasing DFB2 polarization. The maximum observed dynamics range is reached when polarization is 60 degrees, while maximum amplitude was observed with a polarization value of 40 degrees. Also, the maximum number of peaks is observed with the first polarization value. The behaviors are roughly the same, while exact details are changed with selected DFB2 polarization.

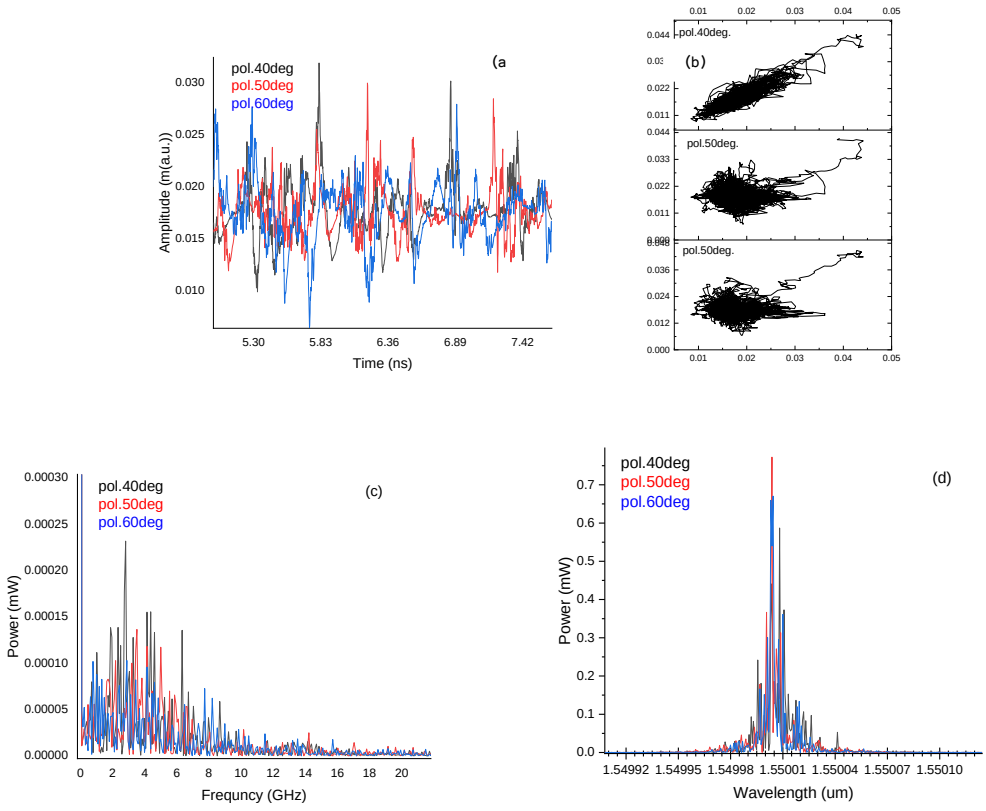

FIGURE 6. Dynamics for summed signal with DFB2 polarzation variation.

(a) Time series (b) Frequency spectrum (c) optical spectrum and (d) phase space.

Table (6). Measurements for FWHM and peak wavelength against phase shift for received signal from the influencer given in figure (6).

Polarization (degree)	Dynamics range (GHz)	No. of peaks	λ_p(um)	
			Lambda (um)	Power (mW)
40	0-10	15	1.54999573	0.234658515
			1.55000836	0.369988813
			1.55000375	0.441007127
			1.55000864	0.58769338
50	0-15	16	1.5500005	0.36612173
			1.55000906	0.308070906
			1.55000331	0.778364703
60	0-16	24	1.54999659	0.159397308
			1.55001018	0.347935965
			1.55000308	0.649175429
			1.55000462	0.670262298

Effect of DFB3 in overall summed signal

Also effect of DFB3 on the last follower laser was investigated, regardless of DFB1 and DFB2, and by changing the polarization for (70-80) degree, Fig. 7. Polarizations of the first and second lasers are fixed on (30-60), respectively. Analysis is listed as values for signal dynamics and shown in Table 7. Dispute to weight of DFB2 in summed signal, number of peaks decreases with increasing polarization. An important observation is that in the case of reviewing the results for the outbreak, resulted signal with polarization value of (90). the signal is a straight line and where the electric vehicle was canceled, while after collecting the signals, the result is not a straight line free of Peaks, we noticed the appearance of a number of pikes, and this is due to the laser effect on the other after the collection process.

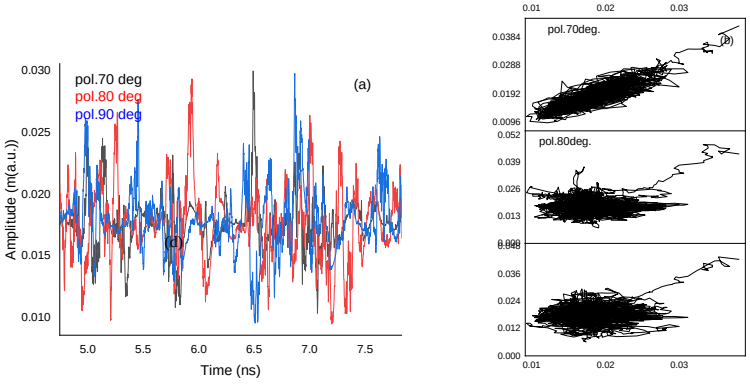

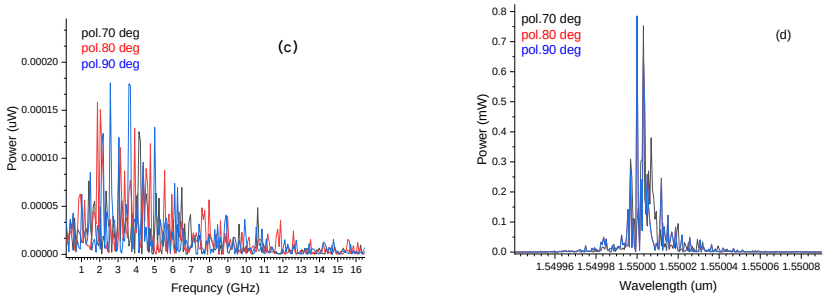

FIGURE 7. Dynamics for summed signal with DFB3 polarzation variation.
(a) Time series (b) Frequency spectrum (c) optical spectrum (d) phase space

Table (7). Measurements for FWHM and Peak wavelength against phase shift for received signal from the influencer given in figure (7).

Polarization (degree)	Dynamic range (GHz)	No. of peaks	λ_p(um)	
			Lambda (um)	Power (mW)
70	0-11	12	1.54999702 1.5500069 1.55000307	0.303431185 0.37035252 0.752451759
80	0-13	16	1.55001177 1.54999696 1.55000333 1.54999989	0.245879658 0.273869459 0.652541405 0.800123996
90	0-12	11	1.55001231 1.55000356 1.55000013	0.244934678 0.647491103 0.806845747

Dynamics with follower laser modulation with optical amplification EDFA 5m

In this part, the polarization value is selected at 30–60–90 degrees for the three influencers lasers, respectively. The modulation value on the follower laser was swept by the signal generator for a specific range. At first, a chaotic signal is observed, then the signal is converted to a periodic, i.e., coherent, waveform (Fig. 8). Statistics for swept values are listed in Table 8. The observed chaotic signal results in a value of 119MHz. While there is a point of inversion at 120 MHz, the signal changes from chaotic to periodic where it appears periodic. Also, it is noticed from the last table that the number of peaks begins to increase until the value reaches 120 MHz for periodic signals. Thus, there are no more peaks observable. Attractors also adapt the last observation in phase space. Many studies, such as Ref. [37] and others, utilized light's various degrees of freedom, such as wavelength, polarization, diffraction order, orbital angular momentum, etc., to provide applications for data encryption, display, and information processing. With such a technique the sent order will be masked during its trip toward its terminal, the same idea applicable with signal that carried out inside processors for artificial intelligence.

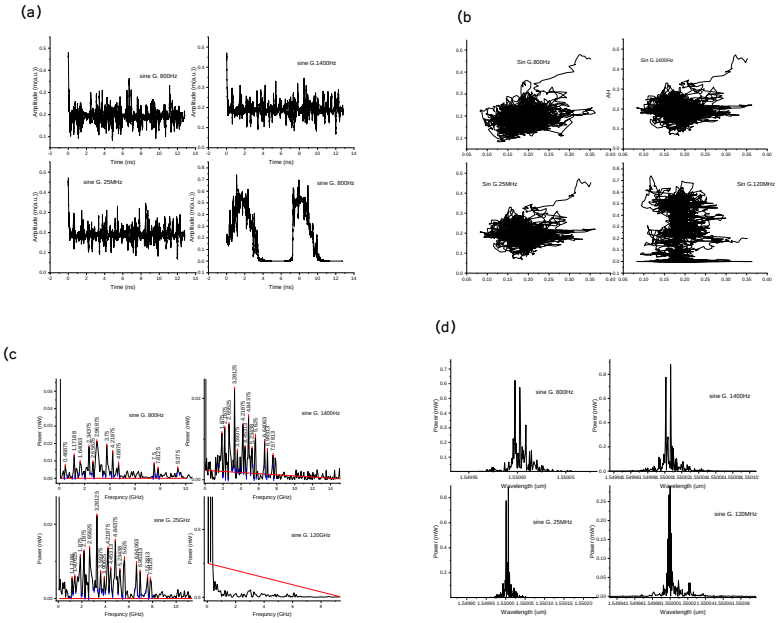

FIGURE 8. Dynamics for summed signal after modulation and amplification. (a) Time series , (b) Frequency spectrum, (c) optical spectrum and (d) phase space

Table (8). Measurements for FWHM and Peak wavelength against phase shift for received signal from the influencer given in figure (8).

Modulated frequency value	Dynamics range (GHz)	No. of peaks	λ_p(um)	
			Lambda (um)	Power (mW)
800 Hz	0-10	12	1.55000863 1.55000254 1.54999751	0.315269519 0.57828569 0.626639638
1400 Hz	0-8	13	1.5500014 1.55000683	0.775705412 0.88424012
25 MHz	0-9	17	1.55000129 1.55000659	0.782912969 0.886945299
120 MHz	0-6	0	1.55002276 1.54999983	0.0375689838 0.290914366

III.CONCLUSION

A network of three lasers can be connected in such a way to interchange variety of coded signals via chaotic masking. Since laser active medium is considered to confirm a single input layer operation, it is necessary to represent suitable non-linear activation functions for machine learning. The effect of polarization can be used as a control parameter to evaluate the weight of each signal in this layer. Observation indicated nearly identical behaviors with different detailed spectra for each influencer laser source. At a value of 120 MHz, the signal was converted from chaotic to periodic which means that there is a critical modulation value for keep signal masked. This is due to the effect of injection in the feed-forward regime, which leads to an overlap between the laser cavity frequency and the frequencies coming from the injection in addition to the summed frequencies. All interacted and led to several different signals.

The simulation outcomes demonstrate that our network structure is capable of successfully sorting three different types of orthogonally polarized vortex beams to demultiplexing hybrid beams into Gauss beams at three spatial places, versus investigated polarizations.

ACKNOWLEDGMENTS

The authors would like to thank Mustansiriyah University, (www.uomustansiriyah.edu.iq) Baghdad – Iraq for their support.

IV. REFERENCES

[1]. R. Hamerly, L. Bernstein, A. Sludds, M. Soljačić and D. Englund, "Large-Scale Optical Neural Networks Based on Photoelectric Multiplication," Physical Reviewx, vol. X 9, no. 021032, pp. 1-12, 2019. 10.1103/PhysRevX.9.021032.

[2]. H. J. Caulfield and R. S. K. J Kinser, "Optical Neural Networks," in Proceedings of the IEEE, vol. 77, no. 10, pp. 1573-1583, Oct. 1989, doi: 10.1109/5.40669., 1989..

[3]. I. A. D. Williamson, T. W. Hughes, M. Minkov, B. Bartlett, S. Pai and S. Fan, "Reprogrammable Electro-Optic Nonlinear Activation Functions for Optical Neural Networks," IEEE Journal Of Selected Topics In Quantum Electronics, vol. 26, no. 1, pp. 1-12, pp. 7700412-7700412, 2020. 10.1109/JSTQE.2019.2930455.

[4]. L. M. Zhang and J. E. Carroll, "Large-Signal Dynamic Model of the DFB Laser," IEEE Journal Of Quantum Electronics, vol. 28, no. 3, pp. 604-611, pp. 604-611, 1992. 10.1109/3.124984.

[5]. W. Liu, Z. Wang, X. Liu, N. Zeng, Y. Liu and F. E. Alsaadi, "A survey of deep neural network architectures and their applications," Neurocomputing, Vols. 234 pp. 11-26, pp. 11-26, 2017. https://doi.org/10.1016/j.neucom.2016.12.038.

[6]. A. A. Hemed, Chaos Generation Methods in Optical Communication Systems, Baghdad: University of Baghdad, 2011.

[7]. Y. Zhao, J. Gao and Xuezhi Yang, "A survey of neural network ensembles," Beijing, 2005. 10.1109/ICNNB.2005.1614650.

[8]. H. Kukreja, B. N, S. C and K. S, "An Introduction to Artifical Neural Network," Ijariie-ISSN, vol. 1, no. 5, pp. 27-30, 2016. https://www.researchgate.net/profile/Kuldeep-Shiruru/publication/319903816_AN_INTRODUCTION_TO_ARTIFICIAL_NEURAL_NETWORK/links/59c0fe55458515af305c471a/AN-INTRODUCTION-TO-ARTIFICIAL-NEURAL-NETWORK.pdf.

[9]. W. Zheng and G. W. Taylor, "Determination of the Photon Lifetime for DFB Lasers," IEEE Journal of Quantum Electronics, vol. 43, no. 4, pp. 295-302, p. 295, 2007. 10.1109/JQE.2006.889746.

[10]. A. A. Hemed, Z. R. Ghayib and H. G. Rashid, "Controlling a chaotic anti-synchronized oscillator by a phase interplayed optical injected seed with an FBG sensor," in 2nd International Conference on Physics and Applied Sciences (ICPAS 2021) College of Education, Mustansiriyah University, Baghdad, Iraq, 26-27 MAY, 2021. 10.1088/1742-6596/1963/1/012063.

[11]. D. R. Madhloom, A. A. Hemed and S. M. Khorsheed, "Experimental Simulation for Two Optically Filtered Modulation Weights in Laser Diode as a Self-Learning Layer," 2023.

[12]. R. S. Abbas and A. A. Hemed, "Hyper chaos and anti-synchronization by dual laser diode," 2023.

[13]. A. D. Dongare, R. R. Khard and A. D. , "Introduction to Artificial Neural Network," International Journal of Engineering and Innovative Technology (IJEIT), vol. 2, no. 1, pp. 189-194, 2012. https://citeseerx.ist.psu.edu/document?repid=re

p1&type=pdf&doi=04d0b6952a4f0c7203577afc9476c2fcab2cba06.

[14]. P. M. AtkInson and A. R. L. Tatnall, "Introduction Neural networks in remote sensing," INT.J. Remote Sensing, vol. 18, no. 4, pp. 699-709, 1997. https://doi.org/10.1080/014311697218700.

[15]. K. Güney, M. Erler and S. Sagiroglu, "Artificial Neural Networks for the Resonant Resistance Calculation of Electrically Thin and Thick Rectangular Microstrip Antennas," Electromagnetics, Vols. 20, 2000, pp. 387-400, no. 5, pp. 387-400, 2000. https://doi.org/10.1080/027263400750064392.

[16]. A. D. Dongare, R. R. Kharde and A. D Kachare, "Introduction to Artificial Neural Network," International Journal of Engineering and Innovative Technology (IJEIT), vol. 2, no. 1, pp. 189-194, 2012. https://citeseerx.ist.psu.edu/document?repid=rep1&type=pdf&doi=04d0b6952a4f0c7203577afc9476c2fcab2cba06.

[17]. K. Kojima, K. Kyuma and T. Nakayama, "Analysis of the Spectral Linewidth of Distributed Feedback Laser Diodes," Journal Of Lightwave Technology, vol. 3, no. 5, pp. 1048-1055, 1985. 10.1109/JLT.1985.1074295.

[18]. E. Rønnekleiv, M. N. Zervas and J. T. Kringlebotn, "Modeling of Polarization-Mode Competition in Fiber DFB Lasers," IEEE Journal Of Quantum Electronics, vol. 34, pp. 1559-1569, 1998. 10.1109/3.709571.

[19]. A. Lowery and BSc, "New dynamic semiconductor laser model based on the transmission-line modelling method," IEE Proceedings, vol. 134, pp. 281-290, 1987. 10.1049/ip-j.1987.0047.

[20]. E. Rønnekleiv, M. Ibsen and G. J. Cowle, "Polarization Characteristics of Fiber DFB Lasers Related to Sensing Applications," IEEE Journal Of Quantum Electronics, vol. 36, pp. 656-664, 2000. 10.1109/3.845719.

[21]. T. Fessant and Y. Boucher, "Additional Modal Selectivity Induced by a Localized Defect in Quarter-Wave-Shifted DFB Lasers," IEEE Journal Of Quantum Electric, vol. 34, no. 4, pp. 602-608, pp. 602-608, 1998. 10.1109/3.663433.

[22]. K. Yelen, L. M. B. Hickey and M. N. Zervas, "A New Design Approach for Fiber DFB Lasers With Improved Efficiency," IEEE JOURNAL OF QUANTUM ELECTRONICS, vol. 40, pp. 711-720, 2004.10.1109/JQE.2004.828257.

[23]. R. Rudra, A. Biswas, P. Dutta and G. Aarthi, "Applying regression models to calculate the Q factor of multiplexed video signal based on Optisystem," 2015. 10.1109/IntelliSys.2015.7361145..

[24]. N. K. Grady, J. E. Heyes, D. R. Chowdhury, Y. Zeng, M. T. Reiten, A. K. Azad, A. J. Taylor, D. A. R. Dalvit and H.-T. Chen, "Terahertz Metamaterials for Linear Polarization Conversion and Anomalous Refraction," Reports, vol. 340, no. 6138, pp. 1304-1307, 2013. 10.1126/science.1235399.

[25]. I. Amiri, A. N. Z. Rashed, H. M. A. Kader, A. A Al-Awamry, I. A. A. El-Aziz, P. Yupapin and G. Palai, "Optical Communication Transmission Systems Improvement Based on Chromatic and Polarization Mode Dispersion Compensation Simulation Management," Journal Pre-proof, vol. 207, no. 163853, pp. 1-9, 2020. https://doi.org/10.1016/j.ijleo.2019.163853.

[26]. W. Zheng and G. W. Taylor, "Determination of the Photon Lifetime for DFB Lasers," IEEE Journal Of Quantum Electronics, vol. 43, no. 4, pp. 295-302, pp. 295-302, 2007. 10.1109/JQE.2006.889746.

[27]. B. F. Kennedy, F. Surre, S. Philippe, L. Bradley and P. Landais, "The Use Of Polarization Efeects In Semicondutor Optical Amplifers To Perfom All-Optical Signal Processing," Ingeniare. Revista chilena de ingeniería, vol. 15, no. 3. pp. 313-319, pp. 313-319, 2007. https://www.redalyc.org/pdf/772/77215311.pdf.

[28]. P. Morin, S. Pitois and J. Fatome, "Simultaneous polarization attraction and Raman amplification of a light beam in optical fibers," Journal of the Optical Society of America B, Vols. 29, Issue 8, pp. 2046-2052, no. 8, pp. 2046-2052 , pp. 2046-2052, 2012. https://opg.optica.org/josab/abstract.cfm?uri=josab-29-8-2046.

[29]. J. M. Pol, Polarization and Intensity Noise in Vertical-Cavity Surface-Emitting Lasers, Palma, 2001.

[30]. M. Guasoni, P. Morin, P.-Y. Bony, S. Wabnitz and J. Fatome, "Self-induced polarization tracking, tunneling effect and modal attraction in optical fiber," Optics and Laser Technology, Vols. 80, pp. 247-259, pp. 247-259, 2016. https://doi.org/10.1016/j.optlastec.2015.12.011.

[31]. S. L. Chuang, Physics of Photonic Devices, 2nd Edition, 2nd ed. Wiley: Wiley, 2009.

[32]. A. J. Lowery, "New dynamic model for multimode chirp in DFB semiconductor lasers," IEE Proceedings, vol. 137, p. 293, 1990.https://ui.adsabs.harvard.edu/abs/1990IPOpt.137..293L/abstract.

[33]. G. Zhao, J. Sun, Y. Xi, D. Gao, Q. Lu and W. Guo, " Design and simulation of two-section DFB lasers with short active-section lengths," Optics Express, vol. 24, no. 10, pp. 10590-10598, 2016 . https://doi.org/10.1364/OE.24.010590.

[34]. A. A. Hemed, Study the effect of Birefrengence (High and low) in a single mode optical fiber, Baghdad: College of education, Mustansiriyah University, 2005.

[35]. J. Zhang, Z. Ye, J. Yin, L. Lang and S. Jiao, "Polarized deep diffractive neural network for sorting, generation, multiplexing, and de-multiplexing of orbital angular momentum modes," Optics Express, vol. 30, no. 15, pp. 26728-26741, 2022•https://doi.org/10.1364/OE.463137.

[36]. J. Li, Y.-C. Hung, O. Kulce, D. M. Ozcan and A. Ozcan, "Polarization multiplexed diffractive computing: all-optical implementation of a group of linear transformations through a polarization-encoded diffractive network," Light Sci Appl, vol. 11, no. 153, pp. 405-408, 2022. https://doi.org/10.1038/s41377-022-00849-x.

[37]. G. G. Q. W. Ruizhe Zhao, Y. Liu, H. Zhou, X. Zhang, C. He, X. Li, X. Li, Y. Wang, J. Li and L. Huang, "Controllable Polarization and Diffraction Modulated Multi-Functionality Based on Metasurface," Advanced optical materials, vol. 10, no. 8, 2022. https://doi.org/10.1002/adom.202102596.

Cite this article as :

Mariam R. Dhyaa, Ayser A. Hemed, "Effect of input layer signal polarization on the dynamics of optical neural networks", International Journal of Scientific Research in Science, Engineering and Technology (IJSRSET), Online ISSN : 2394-4099, Print ISSN : 2395-1990, Volume 10 Issue 5, pp. 279-293, September-October 2023. Available at doi : https://doi.org/10.32628/IJSRSET2310543
Journal URL : https://ijsrset.com/IJSRSET2310543